# ANALYSIS OF RELATIVE PERFORMANCE AMONG NUMERICAL METHODS APPLIED TO THE THIN PLATE THEORY

**Vitor Pancieri Pinheiro**

**Carlos Friedrich Loeffler**

**Natan Sian das Neves**

**Daniel Carvalho de Moura Candido**

vitor.pinheiro1987@gmail.com

carlosloeffler@bol.com.br

natan.sian@gmail.com

danielcandido89@gmail.com

Programa de Pós-Graduação da Universidade Federal do Espírito Santo - UFES – Centro Tecnológico – Av. Fernando Ferrari, 540 – Bairro Goiabeiras – 29075 – 910, Vitoria, ES – Brasil.

***Abstract.*** *In the broad context of mathematical-physics, the thin plate theory presents itself as a model of great relevance due to its applicability in structural engineering, which justifies the volume of current research on the subject. In this context, choosing the most effective numerical method for solving an arbitrary mathematical model is of vital importance to increase result effectiveness in a project. This work focuses on a relative efficiency analysis between the boundary element method, finite element method and also the finite difference method, applied to rectangular plate simple supported with different loading conditions. It is intended, therefore, to draw a systemic parallel between the methods in order to quantify the performance of each of them in the proposed problem. Finally, the absolute performance evaluation is based on comparisons with known analytical solutions available in the literature.*

***Keywords:*** *Thin Plate Theory, Numerical Methods, Systemic Comparison*

# 1 INTRODUCTION

Among the various structural elements used in the engineering field , plates stand out for the wide versatility of application, in the form of slabs, elements of sealing in buildings, diverse components of aeronautical fuselages, besides recurring use in the naval industry and in the composition of machines. The design and analysis of plates has three fundamental approaches, being they the theoretical modeling and empirical and numerical experimentation. The focus of this paper, therefore, is based on the analysis and comparison of performance through simulations via numerical methods widely diffused in engineering.

In general, each numerical method has particularities regarding the treatment of the theoretical model, which varies according to the nature of its formulation, which may be integral or differential. Methods of differential nature are characterized by the direct execution of the discretization process on the differential equation of government, while integral methods require the elaboration of an equivalent integral sentence of the phenomenon, and then, afterwards, the transference to the discrete medium is carried out.

In the context of differential numerical methods, the strength of the finite difference method (FDM) is emphasized as a precursor in the numerical analysis of engineering problems, and still widely used due to the simplicity of its formulation and application. In the scope of integral methods, the finite element method (FEM), whose versatility and robustness in the formulation makes it a recurring choice in the development of programs at commercial level. Finally, more recently, the boundary element method (BEM) has been gaining space in the scientific environment due to its good performance in several models of interest, emphasizing advantages such as the treatment of the boundary of the domain only, in order to simplify calculations by reducing the dimensions under analysis. The three methods are applied here to the deformational analysis of plates, in order to infer about the most efficient option for the physical application in question, limited to previously fixed parameters.

# 2 MATHEMATICAL MODEL

The Thin-Plate Theory aims to mathematically model the behavior of loaded plates by means of a differential equation. Based on the theory of elasticity, this classical theory assumes that the analyzed materials are perfectly elastic linear, homogeneous and isotropic. It is further considered that there is no deformation in the median plane of the plate and that sections initially transverse to this plane remain orthogonal to the deformed surface of the plate after deformation. In addition, the compression stresses perpendicular to the surface are disregarded due to the small thickness in relation to the other dimensions, which configures classic characteristic of the thin plate formulation (Reddy, 2006).

The differential model that represents the behavior of a thin plate under a load $q$ is deduced from concepts of the analysis of linear structural parts adapted for a surface element under pure bending. The fourth-order partial differential governing equation representing the core of the thin-plate theory is shown below in Eq. (1).

$$\nabla^4 w = \frac{q}{D} \qquad\qquad D = \frac{Eh^3}{12(1-\nu^2)} \tag{1}$$

Once the appropriate boundary conditions have been defined, the solution of Eq. (1) determines the deformation surface $w(x, y)$ of a plate subjected to a generic loading $q$, whose mechanical and geometric characteristics are accounted for in the flexural rigidity modulus $D$. The flexural rigidity varies according to the thicknesses ($h$) of the plate, the longitudinal modulus of elasticity ($E$) and the Poisson's coefficient ($\nu$) of the constituent material of the analyzed element.

$$\nabla^2(\nabla^2 w) = \frac{q}{D} \tag{2}$$

The differential governing equation can also be expressed for cases restricted to simply supported by a fourth-order differential operator decomposition of Eq. (1) on two Laplace operators as given by Eq. (2). Such partitioning of the problem requires the solution of a first differential expression given by Eq. (3), whose primal variable is the bending moment and the domain load is characterized by the loading itself acting on the plate (Timoshenko & Woinowsky-Krieger, 1959).

$$\frac{\partial^2 M}{\partial x^2} + \frac{\partial^2 M}{\partial y^2} = -q \tag{3}$$

In sequence, the solution of a second differential equation, expressed by Eq. (4), is required, in terms of the deflection at each point of the plate as the primal variable, and the internal bending moment loading from the solution of Eq. (3) as a domain load, less than one constant, $D$.

$$\frac{\partial^2 w}{\partial x^2} + \frac{\partial^2 w}{\partial y^2} = \frac{-M}{D} \tag{4}$$

Since the boundary conditions are known for moments $M$, in Eq. (3), it can be solved and the calculated values are then replaced as domain load to solve Eq. (4), where it is necessary that the boundary conditions $w$ be known. Therefore the dismemberment shown is limited to cases of plates simply supported on the four edges.

## 2.1 Analytical Solution: Partially Loaded Plate

The complexity of the mathematical model presented by the thin-plate theory makes it difficult to develop a general solution of Eq. (1), so a great research effort was made in the elaboration of approximate solutions for specific cases of loadings and boundary conditions. In this line, satisfactory solutions were produced by the representation of the differential equation and the load in terms of series of harmonic functions illustrated in this section.

The plate illustrated in Fig. 1 with length $a$ and width $b$, simply supported at all ends is subject to a load $Q$ symmetric to the axes $x$ and $y$ and is uniformly distributed in the hatched area of sides $u$ and $v$.

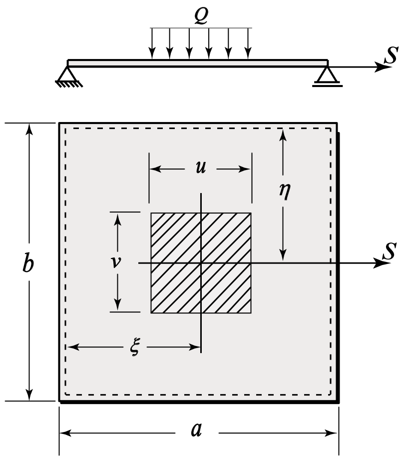


**Figure 1: Schematic of a plate subjected to generalized loading**

A solution for the case of a partially loaded plate, is given by Eq. (5) with its correlated constant in Eq. (6) consisting of a series that converges rapidly in the first terms thereof, as shown in detail by Timoshenko and Woinowsky-Krieger (1959).

$$w = \frac{1}{\pi^4 D} \sum_{m=1}^{\infty} \sum_{n=1}^{\infty} \frac{a_{mn}}{\left(\frac{m^2}{a^2} + \frac{n^2}{b^2}\right)^2} \sin\frac{m\pi x}{a} \sin\frac{n\pi y}{b} \tag{5}$$

$$a_{mn} = \frac{16Q}{\pi^2 mnuv} \sin\frac{m\pi\xi}{a} \sin\frac{n\pi\eta}{b} \sin\frac{m\pi u}{2a} \sin\frac{m\pi v}{2b} \tag{6}$$

The solution presented above is also valid for distributed load across the board if we take $u \to a$ and $v \to b$. The same applies for the case of a load concentrated at the center of the plate for which $u \to 0$ and $v \to 0$.

# 3 NUMERICAL FORMULATION

The current section focuses on a brief description of the numerical formulation of each method to be applied to the Poisson differential model, which arises from the Lagrange equation decomposition, as we have seen previously. This mathematical model is representative of several problems of interest in engineering as in the area of heat transfer, elasticity such as potential flows. The structure of the model, as shown in Eq. (7), consists of a left side which counts the effects of diffusion, and its opposite side representing the source term $f$.

$$-\nabla.(k\nabla u) = f \tag{7}$$

The variable $k$ represents the constitutive tensor, and its treatment strongly determines the complexity associated with the model. In this development, a symmetric, homogeneous and isotropic configuration of the tensor is adopted.

At the conceptual level, classical numerical methods can be classified as the nature of their formulation in integrals and differentials. In general, the differential methods present a logic based on direct approximations of the derivatives in the equation of government. In detriment, the integral techniques set forth herein have a common foundation based on the weighted residual method.

## 3.1 Finite Element Method - FEM

Initially, the finite element method formulation for the classical Poisson equation is presented in the current section. In advance, for the definition of the boundary value problem (BVP), an arbitrary bidimensional domain is considered, in which part of the boundary is subject to the essential condition and the complementary part with natural condition prescription, as summarized below by Eq. (8).

$$\begin{cases} -\nabla.(k\nabla u) = f \\ u = g \quad em \quad \Gamma_g \\ -k\nabla u.\vec{n} = h \quad em \quad \Gamma_h \end{cases} \tag{8}$$

The beginning of the mathematical treatment of the method is by multiplying both sides of the governing equation by an auxiliary function $w$, and the subsequent integration of the equation along the domain of the problem, structuring the so-called strong integral formulation of the problem, as follows in Eq. (9).

$$-\int_\Omega \nabla.(k\nabla u) w d\Omega = \int_\Omega f w d\Omega \tag{9}$$

Then the left-side decomposition of Eq. (9) is applied by piecewise integration, resulting in an integral that continues in the domain and another that can be properly drawn into the boundary by the divergence theorem, a result already computed in the second integral on the left side in the Eq. (10) given below. (Oden & Reddy, 2011).

$$\int_\Omega (\nabla w.k\nabla u) d\Omega - \int_\Gamma w k \nabla u.\vec{n} d\Gamma = \int_\Omega f w d\Omega \tag{10}$$

At this point, it is possible to identify the flux structure associated with the potential field gradient $\nabla u$, in the kernel of the boundary integral of Eq. 10, which can be rewritten and passed to the right side of the integral expression, as shown in the following equation.

$$\int_\Omega (\nabla w.k\nabla u) d\Omega = \int_\Omega f w d\Omega + \int_{\Gamma_h} w h d\Gamma \tag{11}$$

Such integrals are recurrent in the finite element literature and may have their notation simplified, as seen in Hughes (2012). The notation shown below is called the bilinear form of representing structural integrals of the weak integral form. It is important to point out that the latter term represents the prescription of flux in the boundary, and that its natural appearance is due to the very structure of the Poisson equation, which consists conceptually in a liquid flux balance, or in other words the divergent of the flux generated by the gradients of the potential field.

$$a(w,u)_{\Omega} = (w,f)_{\Omega} + (w,h)_{\Gamma_h} \tag{12}$$

In the sequence, it is important to point out that the FEM works with calculations of potentials in all nodes where it is unknown, so that to determine the dimensions of the system it is necessary to know the nodes whose potential is prescribed by essential condition. Thus, in general, one can say that the approximate results of potential $u^h$, can be divided into prescribed potentials, called $g^h$ and potential to be determined by the method, denoted by $v^h$, as synthesized in the expression that follows by Eq. (13).

$$u^h = v^h + g^h \tag{13}$$

Such a consideration allows us to adapt the weak integral formulation to its most definitive format, where the integral containing the function of the potentials to be calculated, shown on the left side of the Eq. (14), has express dependence on the sum of three side effects on the right side of expression, namely, in their respective order, action of the source term in the domain, action of the fluxes imposed in part of the boundary and finally the action of the prescribed potentials in the remaining complementary part of the boundary.

$$a(w^h,v^h)_{\Omega} = (w^h,f)_{\Omega} + (w^h,h)_{\Gamma_h} - a(w^h,g^h)_{\Omega} \tag{14}$$

Once the weak integral formulation is definitively determined by Eq. (14), without any approximation in relation to the initially exposed BVP, it is necessary to subject the formulation to the discretization process. In this respect it is important to note that the Galerkin formulation is chosen for such, where both the unknown potentials $v^h$ and the auxiliary function $w$ are defined as dependent on the same basic functions. In this way, it is possible to prove that the weighting coefficients of the approximation of $v^h$, become the own values of the potentials to be determined, as seen next in Eq. (15).

$$v^h = \sum_{i=1}^{N} u_i \phi_i \qquad w = \phi_i \tag{15}$$

The definitions shown in Eq. (15) can be inserted into the weak integral formulation, resulting in a discretized form whose accuracy depends on the choice of interpolation functions. The discretization process leads to the definition of an elementary coefficient matrix such as a vector of independent terms for each element of the numerical mesh. Once these entities are determined for element, it is possible through a mathematical assembly process, to gather local influences generating a global coefficient matrix, such as a global independent vector.

$$K_{ab}^{e} = \int_{\Omega^e} (\nabla N_a)^T \kappa \, (\nabla N_b) d\Omega \qquad [K] = \mathop{A}_{e=1}^{nel} K^e \tag{16}$$

The integrals of potentials to be determined as well as independent terms are approximated by interpolating polynomials, denoted by $N_a$ and $N_b$. It is possible to see that the expression structure defining the the local stiffness matrix in Eq. (16) is exactly the same as that which defines the global stiffness matrix in the weak formulation put in Eq. (11). In addition it is possible to realize that the elementary independent term depends on three influences: the source term, prescribed potencials and prescribed flux conditions as can be seen in Eq. (14).

$$F_{a}^{e} = \int_{\Omega^e} N_a f d\Omega + \int_{\Gamma^e} N_a h d\Gamma - \sum_{b=1}^{NNP} {k_{ab}}^e g_b^e \qquad [F] = \mathop{A}_{e=1}^{nel} F^e \tag{17}$$

This process culminates in a sparse linear system whose unknowns are the non-prescribed potentials. Such a system can be solved using a wide range of methods oriented to linear systems, whose choice and correct optimization are not part of the scope of this article.

$$[K]\{u\} = [F] \tag{18}$$

## 3.2 Boundary Element Method - BEM

The Poisson differential model is sequentially formulated for a solution using the boundary element method (BEM), which has some mathematical similarity to the FEM, as it is also a method of integral nature, and also very relevant differences for presenting a formulation that discretizes only the boundary of the problem, generating a drastic reduction of complexity in problems with two and three dimensions.

In advance, it is important to mention that the constitutive tensor is omitted here during the mathematical treatment, because it is constant in relation to space by the isotropy and homogeneity of the treated problem. Thus, the beginning of the application of the method is characterized, similar to the FEM, by the multiplication of both sides of the expression of government by an auxiliary function, which in the case of the BEM is the fundamental solution of a problem of the same differential structure in a infinite domain and whose external and punctual excitation is given by a pulse shaped by a Dirac delta. Together, the strong integral formulation can be seen in Eq. (19), while the fundamental solution to the Laplace / Poisson problem, $u*$, in Eq. (20), as following (Brebbia & Dominguez, 1994).

$$\int_{\Omega} u_{,ii}(X) u^*(\xi, X) d\Omega = -\int_{\Omega} f(X) u^* d\Omega \tag{19}$$

$$u^*(\xi, X) = -\frac{1}{2\pi} lnr(\xi, X) \quad (20)$$

A close observation of the strong integral formulation given by the Eq. (19), reveals that the left side is correlated to the Laplace equation, a special case of the Poisson equation, while the right side accounts for the exclusive influence of the source term of the proposed differential model. At this point, another great difference of the BEM with respect to the FEM is highlighted, as regards the integral formulation, since the BEM aims at the integral formulation in its inverse form, while the FEM works with the integral formulation in its weak version. In this context, the inverse formulation associated with the diffusive part represented in the left side in Eq. (19) is widely known in the literature in sources as Brebbia et al. (1984). For this reason, this structure is already shown directly in Eq. (21) which follows.

$$c(\xi)u(\xi) + \int_\Gamma (uq^* - qu^*) d\Gamma = -\int_\Omega f(X) u^* d\Omega \quad (21)$$

Once the left side of the integral formulation is already treated, in its inverse format as seen in the structure immediately above Eq. (21), it is necessary to return the focus to the treatment of the domain integral generated by the influence of the source term, $f(X)$, in the right side of the same equation. In this respect the dual reciprocity formulation will be used to approximate part of the kernel of this integral through radial bases functions and weighting coefficients to be determined. The logic of double reciprocity only calls for the approximation of the source term as shown in the sequence in indicial notation (Partridge et al. 1992).

$$f(X) \cong \alpha^j F^j(X^j; X) = \alpha^j \psi^j{}_{,ii}(X^j; X) \quad (22)$$

The performance of such approaches and the definitions of good choices for radial basis functions are subjects that have been extensively studied and can be seen in more detail in specific literature as in Buhmann (2003). Once the radial basis function to be used is known, it is possible to know its primitive $\psi$, and thus rewrite the domain integral of Eq. (21) by means of this primitive in the following way. Such an integral because it has an analogous structure to the diffusive side already worked, can be taken to the inverse integral format via two successive integrations accompanied by the use of the divergence theorem, resulting in the expression after the equality of the Eq. (23).

$$\alpha^j \int_\Omega \psi^j{}_{,ii}(X^j; X) u^* d\Omega = \alpha^j \left\{ \int_\Gamma \psi_{,i}{}^j n_i u^* d\Gamma - \int_\Gamma \psi^j u_{,i}^* n_i d\Gamma + \alpha^j \int_\Omega \psi^j u_{,ii}{}^* d\Omega \right\} \quad (23)$$

In order to facilitate the representation of the above expression, a parameter $\eta^j$ is defined, which is quantified based on the gradient of the primitive function, such as the flux correlated to the fundamental solution, denoted by $q$ *, as seen below.

$$\eta^j = \psi_{,i}{}^j n_i \qquad q^* = n_i u_{,i}^* \tag{24}$$

The last domain integral on the right side of the Eq. (23) can be determined directly through the properties of the Dirac delta, resulting in a point function correlated to the radial basis function primitive as follows.

$$\alpha^j \int_\Omega \psi^j{}_{,ii}(X^j;X) u^* d\Omega = \alpha^j \left\{ \int_\Gamma \left( \eta^j u^* - \psi^j q^* \right) d\Gamma - c(\xi)\psi^j(\xi) \right\} \tag{25}$$

With such procedures the treatment of the term term related to the source term is complete, via dual reciprocity formulation. At this point, the partial results already discussed by Eq. (21) are assembled together with the final result obtained immediately above by the equation Eq. (25), resulting in the final inverse integral formulation of the boundary value problem in question.

$$c(\xi)u(\xi) + \int_\Gamma (uq^* - qu^*) d\Gamma = -\alpha^j \left\{ \int_\Gamma \left( \eta^j u^* - \psi^j q^* \right) d\Gamma - c(\xi)\psi^j(\xi) \right\} \tag{26}$$

The Eq. (26) is therefore the target of the discretization process, representing the continuous medium by its discrete points results in a matrix system, where the matrix $\alpha$ can be determined from the definition of radial base approximation, allowing the final representation below by the Eq. (27).

$$\{\alpha\} = [F]^{-1}\{f\} \tag{27}$$

A closer observation reveals that the four coefficient matrices present in the Eq. (28) equation arise from the boundary integrals exposed in Eq. (26), where the dot functions on both sides are coupled to the diagonals of the matrices $[H]$.

$$[H]\{u\} - [G]\{q\} = \{[H]\{\psi\} - [G]\{\eta\}\}[F]^{-1}\{f\} \tag{28}$$

Finally, the matrix system above can be conveniently rearranged, where unknown fluxes and potentials can be determined simultaneously.

## 3.3 Finite Difference Method - FDM

The treatment is initiated through finite differences exposing the equation of government in an expanded way, for a clear vision of the differential operators to be approximated. This classical expression has as its mathematical origin in the fundamental principle of energy conservation, which the details can be seen in Reddy (2010).

$$-k\left(\frac{\partial^2 u}{\partial x^2}+\frac{\partial^2 u}{\partial y^2}\right)=f(x,y) \tag{29}$$

According to the philosophy of the method, the derivatives of Eq. (29) are approximated directly, using a scheme of central differences, whose pertinent mathematical details can be found in classical literatures such as Ozisik (1994). The discrete form of the governing equation is shown below by Eq. (30).

$$-k\left(\frac{u_{i+1,j}-2u_{i,j}+u_{i-1,j}}{h_x^2}+\frac{u_{i,j+1}-2u_{i,j}+u_{i,j-1}}{h_y^2}\right)=f_{i,j} \tag{30}$$

In order to better organize and display the discrete equation, also called the finite difference equation, the related coefficients are condensed to the calculation node and its neighboring nodes, in the following format, where the notion of influence of four adjacent nodes in the potential of the current calculation node is clear (Fortuna, 2000).

$$\sigma u_{i,j-1}+\zeta u_{i-1,j}+\Psi u_{i,j}+\lambda u_{i+1,j}+\beta u_{i,j+1}=f_{i,j} \tag{31}$$

The coefficients of the above finite difference equation are given in compact form by Eq. (32), and are restricted to the case of the Poisson model. It is interesting to note that the five coefficients depend only on the constitutive tensor, $k$, of the material and the spacing of the mesh, which leads us to infer about the direct influence of the physical parameters such as the level of mesh refinement in the magnitude and quality of the potentials to be determined. (Szilard, 2004).

$$\Psi=2k\left(\frac{1}{h_x^2}+\frac{1}{h_y^2}\right) \qquad \zeta=\lambda=-\frac{k}{h_x^2} \qquad \sigma=\beta=-\frac{k}{h_y^2} \tag{32}$$

Applying the discretization process, that is, by writing the finite difference equation for each component node of the numerical mesh, a linear system is generated whose coefficient matrix $M$ is written as a function of the constants of Eq. (30), and determined in Eq. (31). The independent term vector $F$ initially only depends on the source term. It is important to note that the matrix structure shown below in Eq. (33) constitutes the pattern of formation for the Poisson problem with the hypotheses of isotropy of the constitutive tensor.

$$M=\begin{bmatrix} \Psi & \lambda & & \beta & & \\ \zeta & \Psi & \ddots & & \ddots & \\ & \ddots & \ddots & \lambda & & \beta \\ \sigma & & \zeta & \Psi & \ddots & \\ & \ddots & & \ddots & \ddots & \lambda \\ & & \sigma & & \zeta & \Psi \end{bmatrix}_{nxn} \qquad F=\begin{bmatrix} f_1 \\ \vdots \\ f_n \end{bmatrix} \tag{33}$$

Finally, to characterize the BVP, the boundary conditions are imposed, and they specifically change the matrix $M$ and the vector of independent terms $F$, depending on the type of prescribed boundary condition, each with its correlated actions, conforms can be seen in greater detail wealth in Ozisik (1994). The final linear system, after the particularization of the problem, second the conditions imposed on the BVP is given below by the Eq. (34).

$$[M']\{u\} = [F'] \tag{34}$$

# 4 RESULT ANALYSES

With the purpose of performing a valid comparison, it is convenient to establish a methodological sequence justified by pertinent literature and the fundamental philosophy of each numerical method. In this context, it is necessary to highlight the difficulties present in the comparison of numerical methods with a high degree of distinction amongst them, as is the case with the FDM, BEM and FEM. To demonstrate such differences, observe the three two-dimensional square meshes in the figure below.

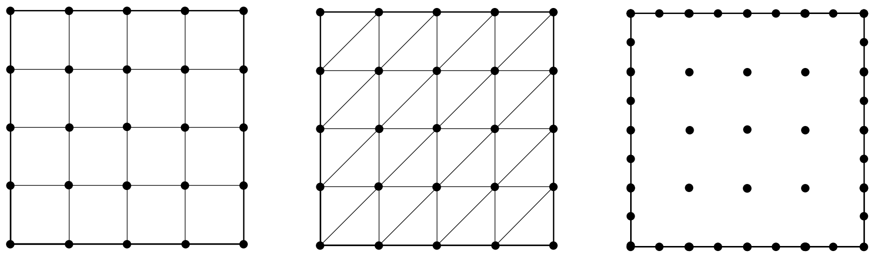

**Figure 2: General mesh representation for each method.**

The differences in general approach and elaboration of each numerical method become evident when observing, for instance, that the FDM only utilizes the concept of nodes, in a simple and isolated manner. The two integral methods, on the other hand, revolve around the idea of elements over a certain geometry, enclosed by multiple nodes. In this manner, attempts at a comparison between the number of nodes or elements would be frustrated, since it fails to simultaneously consider the mathematical structure and mesh configuration of all three numerical techniques.

In order to appropriately make the considerations mentioned above, the present article proposes the definition of an initial mesh for all three methods, determined as the poorest refinement that wields an average diversion below $1\%$ in comparison with the analytical reference. Although the resulting meshes will contain a different number of nodes and elements for each method, they represent an approximate equivalence of performance for the model analyzed and serve as a starting point for all methods in each analysis performed. Two case studies will be approached with distinct load configurations as represented in Fig 3. Four meshes will be tested for each method, and the refining will consist of approximately doubling the number of nodes in the edges of the domain, starting with the initial mesh configuration determined for each method as specified.

Following the solution of four meshes for each of the three methods, a relative performance analysis will be executed based on the accuracy of results for each node in comparison with the

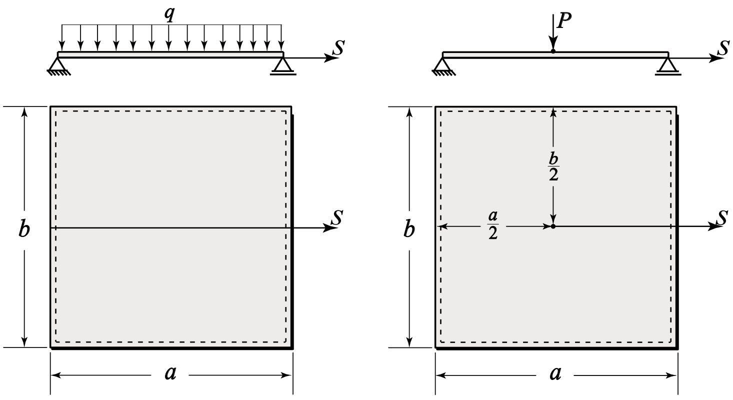


**Figure 3: Esquemas do caso I e II**

analytical solution. The simulations are an attempt to determine which method exhibits the most favorable result when applied to the plate problems with a specific set of properties. The characteristics pertaining to both analyses that will follow are illustrated by Table 1.

**Table 1: Geometric and mechanical properties of the plate**

| Grandeza | Valor | Unidade |
|---|---|---|
| $a$ | 1,0E+00 | m |
| $b$ | 1,0E+00 | m |
| $h$ | 1,0E-01 | m |
| $\nu$ | 2,0E-01 | – |
| $P$ | 1,0E+01 | kN |
| $q_0$ | 1,0E+01 | $\mathrm{kN/m^2}$ |
| $E$ | 3,2E+07 | $\mathrm{N/m^2}$ |

## 4.1 Case I: Uniformly Loaded Plate

The first numerical simulation involve a square plate with sides of unitary length as represented in Fig. 3, subjected to a uniformly distributed load of intensity $q_0$ on its surface. The remaining pertinent properties are represented by Table 1.

The results and respective analyses for all three numerical methods are exposed below, beginning with the finite difference method, applied utilizing the central difference scheme for its mathematical discretization.

The Fig. 4 shows the average error for the finite difference analysis in tabular an graphical formats. A swift rate of convergence for this method can be observed by analyzing the table, as well as a minuscule error percentage with a small amount of degrees of freedom. In addition, The graph shows a monotonic decrease in error percentage as mesh refinement increases, indicating adequate stability for the finite difference method in this case.

Sequentially, the finite element analysis is performed utilizing Galerkin's classical formulation, as explained in previous sections. The result exposition from the FDM is reproduced here, by showing tabular and graphical formats.

| Mesh | Average Error (%) |
|---|---|
| 5 x 5 | 0.306 |
| 10 x 10 | 0.176 |
| 20 x 20 | 0.054 |
| 40 x 40 | 0.015 |

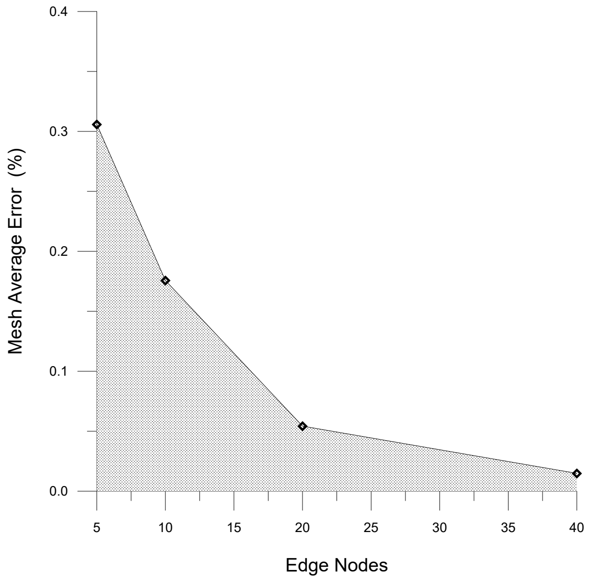


**Figure 4: Convergence Analysis case I - Finite Difference Method**

| Mesh | Average Error (%) |
|---|---|
| 20 x 20 | 0.984 |
| 40 x 40 | 0.238 |
| 80 x 80 | 0.058 |
| 160 x 160 | 0.015 |

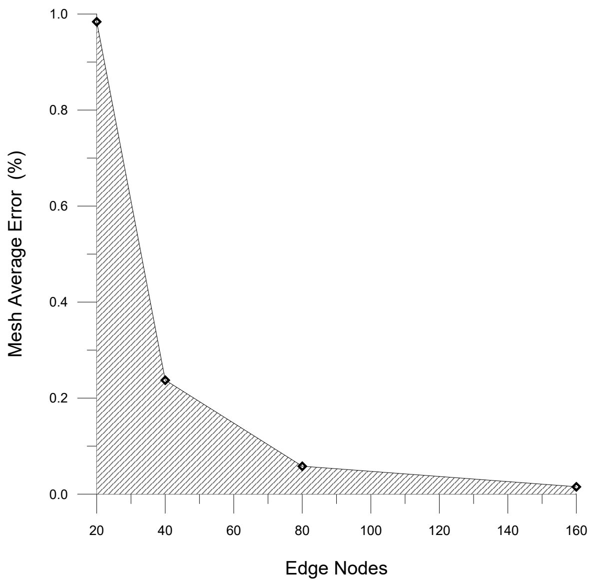


**Figure 5: Convergence Analysis Case I - Finite Element Method**

The table in Fig. 5 shows a satisfactory performance by the FEM, with small errors but a higher demand for degrees of freedom to establish the initial mesh configuration, when compared to the finite difference analysis for this case. The graph shows an inverse relationship between degree of refinement and error percentage, leading to the conclusion that this method also performs well in the first scenario.

The boundary element analysis concludes the first case study. For this application the dual reciprocity BEM was used, as detailed in the numerical formulation. All four meshes for this method were constructed by fixating the number of internal points at $576$, in an attempt to guarantee stability to the formulation.

The data analysis for this case shows that the BEM performs well in the present case, con-

| Mesh | Average Error (%) |
|---|---|
| 64 BE | 0.968 |
| 128 BE | 0.181 |
| 256 BE | 0,160 |
| 512 BE | 0.070 |

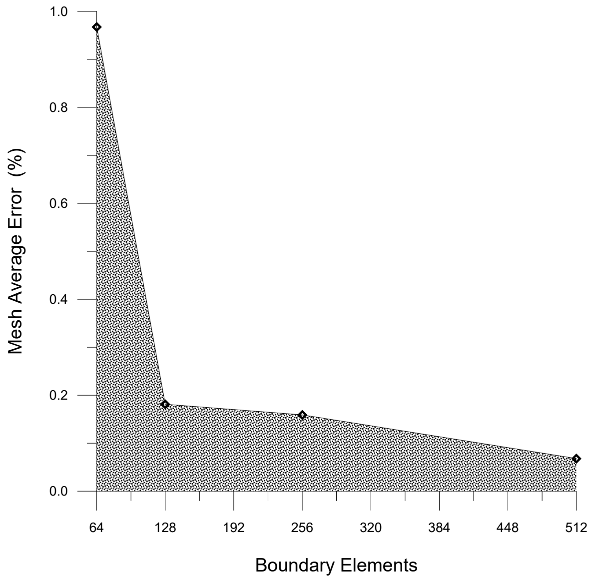


**Figure 6: Convergence Analysis Case I - Boundary Element Method**

tinuing the trend of small error percentages for all meshes, established by the two previous methods. Conversely to the other methods, the boundary element analysis graph does not exhibit a generally monotonic decrease of the error percentage, as the method shows a steeper rate of convergence initially, followed by error stability, this behavior is inherent of the dual reciprocity formulation for the boundary element method.

A general analysis of all three methods for this case brought a few pertinent observations to light. Regarding accuracy, a comparison of the results generated by the meshes with the higher degrees of freedom in all three methods points towards similar performance of the finite difference and finite element methods, however, the FEM demands a significantly higher number of degrees of freedom for the last mesh analyzed, allowing the attribution of the finite difference method as more efficient in this case.

The comparison described between these two methods specifically, is made pertinent by both numerical methods sharing the sparse nature of the system linear of linear equation as a result of their application. In closing this case, the boundary element method exhibits the poorest performance, largely attributed to the nature of the dual reciprocity formulation, notorious for a slower rate of convergence.

## 4.2 Case II: Plate Under Concentrated Load

Subsequently, the second numerical experiment tested also consists of a plate of unitary rectangular dimensions, as shown by Fig. 3, now subjected to a point load $P$ applied at the geometric center thereof. The geometric and mechanical properties of the plate are shown in Table 1.

Analogously to the previous case, the battery of analyzes begins with the exposition of the results presented by the finite difference method, which uses a central spatial discretization scheme in the same way as case I.

The table of Fig 7 again shows a good performance of the finite difference method, which presents recurrent low mean error levels, however, with less pronounced convergence, compared

| Mesh | Average Error (%) |
|---|---|
| 13 x 13 | 0.720 |
| 25 x 25 | 0.174 |
| 49 x 49 | 0.052 |
| 97 x 97 | 0.028 |

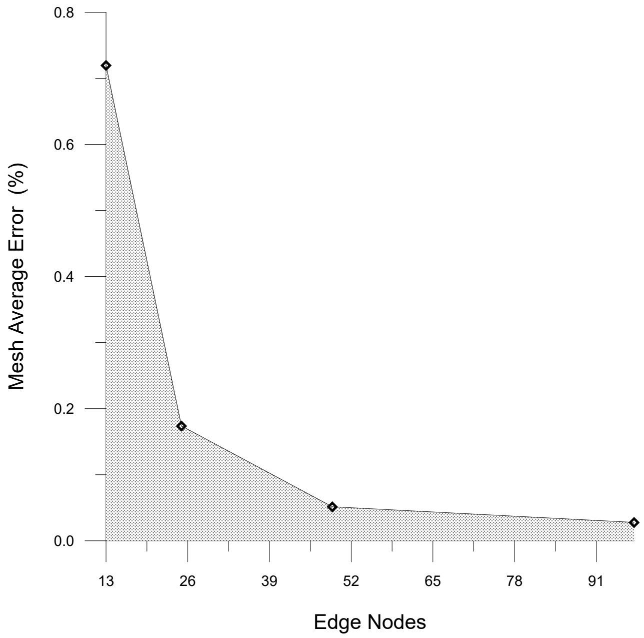


**Figure 7: Convergence Analysis Case II - Finite Difference Method**

to case I. This fact can be duly justified by a higher level of complexity inherent to the nature of the loading of case II, since point loads consist of an idealization of a load applied to regions of area tending to zero. Similarly, the results are synthesized graphically, where a standardized tendency of the fall of the error is observed as the mesh refinement increases.

The results for simulations using the finite element method also formulated with the classical Galerkin proposal, follow below, as seen in previous section.

| Mesh | Average Error (%) |
|---|---|
| 25 x 25 | 0.887 |
| 45 x 45 | 0.229 |
| 89 x 89 | 0.068 |
| 177 x 177 | 0.033 |

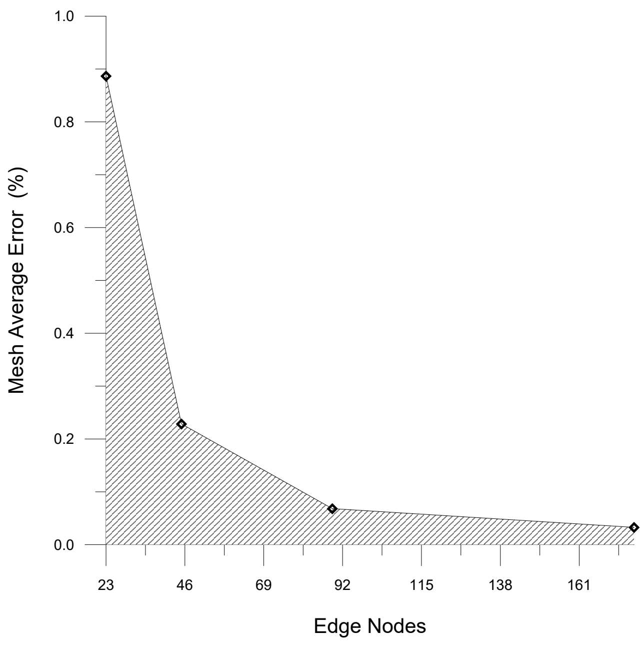


**Figure 8: Convergence Analysis Case II - Finite Element Method**

The results shown in Fig. 8 above demonstrate satisfactory performance of the finite element method in the case in question. It is possible to emphasize that for the current case, the finite difference and finite element method exhibit very similar results, which may be justified by a greater influence of the new loading condition on the finite difference analysis. This fact can be confirmed by comparing the performance of the FEM in case I, in detriment to case II.

In the sequence, and finally, the results of the simulations via boundary elements are presented, where the number of internal points was set at $576$. Analogously to case I, the dual reciprocity formulation is used.

| **Mesh** | **Average Error (%)** |
|---|---|
| 64 BE | 0.785 |
| 128 BE | 0.253 |
| 256 BE | 0.175 |
| 512 BE | 0.145 |

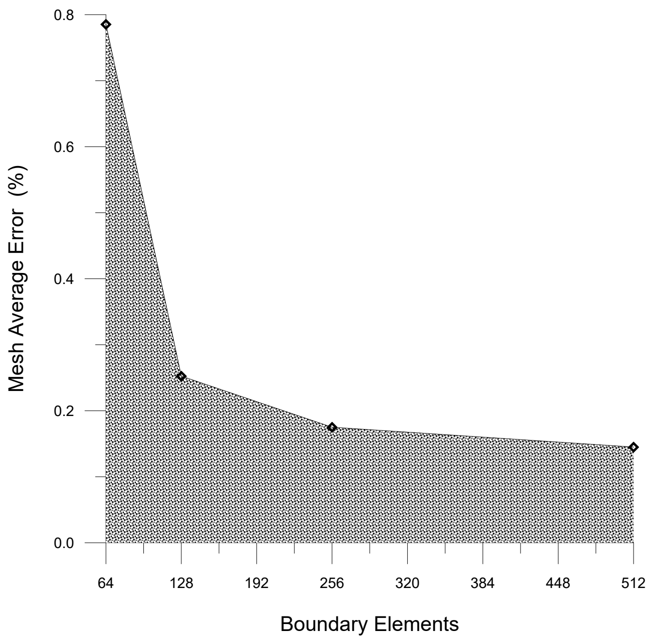


**Figure 9: Convergence Analysis Case II - Boundary Element Method**

Fig. 9, through tabular and graphical format, shows a satisfactory behavior of the BEM, for the problem in question, although clearly inferior to the performance presented by the FDM and FEM. Convergence occurs in an accelerated fashion initially, followed by greater stabilization, as exhibited in the behavior of the previous case, due to the nature of the dual reciprocity formulation.

The general acuity analysis, now for case II, analogous to case I, points out a better performance of the finite difference and finite element methods for the finer mesh configurations, however, the superiority of the FDM is clear. It is possible here to underscore a lower performance disparity between FEM and FDM, which may be justified by the loading model, which more effectively affects the differential method, than the integral FEM formulation based on the weighted residual method. With regard to the boundary element method, we can see a decrease in performance in relation to case I, where once again it presents inferior results to the two others, as a result of the radial bases approach already mentioned in the comments of case I.

# 5 CONCLUSION

In comparative terms, the finite difference method presents the best performance in relation to the other methods in both numerical experiments performed. Despite the similarity to FEM, the superiority of FDM is supported by a lower demand of degrees of freedom to generate similar results. The high efficiency of FDM occurs in large part due to its formulation, more suitable for the treatment of problems with Dirichlet boundary conditions only, as is the case of the models analyzed. The BEM demonstrates the least satisfactory behavior among the techniques tested, which is related to the characteristics of the dual reciprocity formulation applied. On the other hand, it is possible to see a greater sensitivity of FDM associated to load type in each case. Integral methods present greater consistency in the treatment of both loading configurations due to the common grounding associated with the weighted residual method.

The nature of the distributed load in case I, in turn, does not introduce additional complexity to any of the numerical methods tested, and therefore is expected to show better results in this case in detriment to case II, which is fully confirmed. The general performance drop recorded in the second case is caused by the mathematical representation of the load, which is based on the idealization of a load applied on an area that tends to be null. The effectiveness of this loading proposal requires adjustments in the formulation of the methods, which causes considerable accuracy loss, as observed in the tests performed.

The comparison between the numerical methods chosen for the current analysis presents several obstacles originating from the fundamental differences between each of them, from the discretization approach to the nature and application of each formulation. Thus, it is essential that analytical parameters are set in order to minimize the influence of such differences in the comparison of results. The previously performed analyzes used the same boundary conditions with numerical tests starting from meshes that exhibit similar precision and subsequent standard refinement process. These factors corroborate the construction of a satisfactory comparison between the performance of the methods regarding sensitivity to the loading model. Finally, despite the differences in performance between the numerical solutions generated, the three numerical methods present efficient behavior for application in the deformational analysis of thin plates.

## REFERENCES

Reddy, J.N., 2006. *Theory and analysis of elastic plates and shells*. CRC press.

Timoshenko, S.P. and Woinowsky-Krieger, S., 1959. *Theory of plates and shells*. McGraw-hill.

Oden, J.T. and Reddy, J.N., 2011. *An introduction to the mathematical theory of finite elements*. Courier Corporation.

Hughes, T.J., 2012. *The finite element method: linear static and dynamic finite element analysis*. Courier Corporation.

Brebbia, C.A. and Dominguez, J., 1994. *Boundary elements: an introductory course*. WIT press.

Brebbia, C.A., Telles, J.C.F. and Wrobel, L.C., 1984. *Potential problems. In Boundary Element Techniques*. Springer Berlin Heidelberg.

Partridge, P.W., Brebbia, C.A. and Wrobel, L.C., 1992. *The Dual Reciprocity Boundary Element Method*. Computational Mechanics Publication.

Buhmann, M.D., 2003. *Radial basis functions: theory and implementations*. Cambridge University Press.

Reddy, J.N., 2010. *Principles of continuum mechanics*. Cambridge University Press

Ozisik, N., 1994. *Finite difference methods in heat transfer*. CRC press.

Fortuna, A.O, 2000. *Técnicas computacionais para dinâminca dos fluidos: conceitos básicos e aplicações*. Edusp.

Szilard, R., 2004. *Theories and applications of plate analysis: classical numerical and engineering methods*. John Wiley & Sons.